

# Normal and oblique projectile impact of double-layered pyramidal lattice truss structures filled with ceramic insertions

Changye Ni<sup>1,2</sup>, Run Hou<sup>1</sup>, Bin Han<sup>1</sup>, Feng Jin<sup>1</sup>,  
Guwei Ma<sup>2,3</sup> and Tianjian Lu<sup>1</sup>

## Abstract

Systematic three-dimensional finite element (FE) simulations are carried out to study the ballistic protection performance of double-layer sandwich plates having metallic pyramidal lattice truss cores filled with ceramic prism insertions and void-filling epoxy resin. Both normal and oblique projectile impacts are considered in the FE simulations that are validated against experimental measurements. The ballistic limit velocity, the energy absorbed by key constituting elements and the critical oblique angle corresponding to the transition from ballistic perforation to projectile embedment are calculated. As the oblique angle is increased, the evolution of deformation and failure in the double-layer plates as well as the underlying mechanisms are explored. It is demonstrated that the proposed double-layer sandwich plates outperform both the single-layer sandwich plates and the homogeneous (monolithic) metallic plates having equal total mass, and the top layer (the ceramic insertions in particular) of the double-layer configuration plays a more dominant role in energy absorption.

## Keywords

Layered structures, hybrid-cored sandwich, impact behaviour, energy absorption, finite element analysis (FEA)

<sup>1</sup> State Key Laboratory for Strength and Vibration of Mechanical Structures, Xi'an Jiaotong University, Xi'an, People's Republic of China

<sup>2</sup> School of Civil, Environmental and Mining Engineering, The University of Western Australia, Crawley WA, Australia

<sup>3</sup> College of Architecture and Civil Engineering, Beijing University of Technology, Chaoyang, Beijing, People's Republic of China

## Corresponding author:

Tianjian Lu, State Key Laboratory for Mechanical Structure Strength and Vibration, Xi'an Jiaotong University, Xi'an 710049, People's Republic of China.

Email: tjlu@mail.xjtu.edu.cn

## Introduction

The concept of layered plates has been explored in order to enhance the ballistic perforation resistance over a monolithic plate (often made of high-strength steel).<sup>1</sup> The ballistic resistance of layered steel plates (both with and without spacing) struck by 7.62 mm standard bullets was investigated experimentally by Almohandes et al.<sup>2</sup> A single steel plate was found to be more effective than a layered plate of an equal total thickness and the perforation resistance of layered plates increased as the number of plates decreased and the thickness of the back plate increased with the same total thickness. Using a combined experimental and numerical approach, Gupta et al. investigated the behaviour of thin layered aluminum plates of different thicknesses under the impact of flat, ogival and hemispherical steel projectiles. For the double-layered plates, the residual velocity of the projectile was found to be comparable to that of a single plate of equivalent thickness.<sup>3</sup> When the number of layers was increased, however, the single plate offered more resistance against perforation which is consistent with the result of Almohandes et al.<sup>2</sup> However, Teng et al. studied numerically the protection performance of double-layered metal shields against blunt and conical-nose projectiles impact and found the double-layered targets exhibited advantage over monolithic plates of equal weight.<sup>4</sup>

In addition to layered plates, to increase the ballistic resistance of monolithic plates, lightweight sandwich constructions having highly porous two-dimensional) or three-dimensional (3D) periodic metallic lattice truss cores were investigated.<sup>5-9</sup> For example, ceramic prisms were inserted into the interstices of pyramidal lattice trusses to construct pyramidal-ceramic hybrid-cored sandwich plates to increase the performance of empty pyramidal lattice truss structures under projectile impact.<sup>10,11</sup> It was demonstrated both experimentally and numerically that the sandwich plates with pyramidal-ceramic-epoxy hybrid core as illustrated schematically in Figure 1(a) possessed superior ballistic resistance and energy absorption capability over those without ceramic inserted or epoxy infiltrated as well as a monolithic metal plate having an equal total mass. Whilst the projectile was severely eroded by the ceramic insertions, the infiltrated epoxy resin adhered all the sub-structures as an integrated whole, thus improving significantly the energy absorption capacity of the hybrid-cored sandwich structure.<sup>11</sup> It was also shown that, with a certain total mass of the sandwich structure, decreasing the thickness of its front face-sheet whilst increasing that of the back face-sheet could enhance further its ballistic protection capability.<sup>11</sup> Bazle Z (Gama) et al. also presented a combined theoretical-semiempirical penetration model of ballistic penetration of thick section composites.<sup>12</sup> Shanazari H et al. developed an analytical model based on wave propagation and energy balance between the projectile and target to analyze hybrid fabric panels for ballistic protection.<sup>13</sup> Tasdemirci A et al. discussed the effect of interlayer on the damage formation in a ceramic/composite armour.<sup>14,15</sup> The effect of interlayer which can reduce stress wave transmission was demonstrated experimentally and numerically.

Existing studies of layered metal plates or hybrid-cored sandwich constructions focussed mainly upon the most critical impact condition, namely, the normal impact case

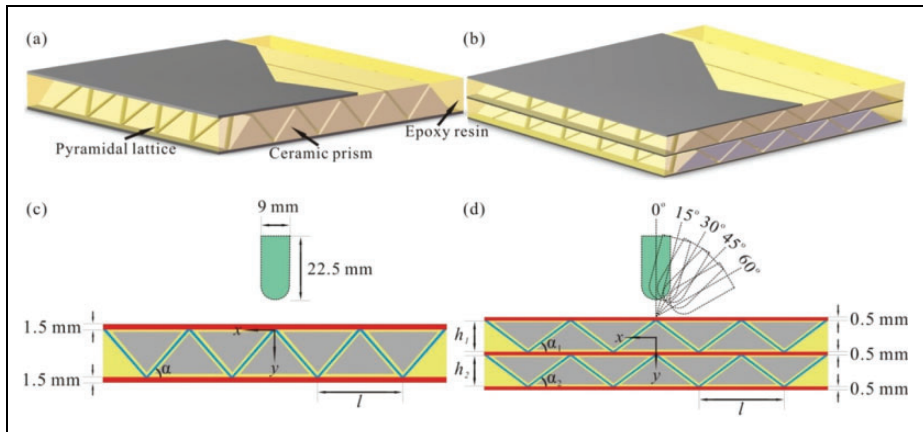


**Figure 1.** Schematic of (a) single-layer and (b) double-layer sandwich plate having metallic pyramidal lattice truss core filled with ceramic prisms and epoxy resin. Hemispherical projectile (bullet) impacting plate center at (c) normal angle and (d) oblique angle.

where the projectile impacts the target perpendicularly. However, the oblique angle of a projectile affected not only the penetration depth and energy absorbed but also its deformation/failure modes of the target.<sup>16–21</sup> In general, the penetration resistance of the target increases with increasing angle of obliquity. In the present study, double-layered sandwich plates having pyramidal-ceramic-epoxy hybrid cores as shown in Figure 1(b) are constructed and their ballistic performance under normal projectile impact is examined with numerical simulations. The aim is to investigate whether the layered sandwiches can enhance further the ballistic performance of a single-layered sandwich. The effect of oblique projectile impact on the ballistic resistance of these double-layered sandwiches is quantified and the critical oblique angle at which the penetration process changes from perforation to embedment is identified. The accuracy of the numerical simulations is verified against experimental measurements under normal ballistic impact.

## Problem description

With reference to Figure 1(a) and (b), consider both single- and double-layered sandwich plates having metallic pyramidal lattice truss cores filled with ceramic prisms and epoxy resin. The hybrid-cored sandwich plates are clamped and shot by a hemispherical projectile at the plate center. Both normal and oblique impact conditions are considered, as shown schematically in Figure 1(c) and (d), respectively.

For the single-layered plates,  $\alpha$  denotes the inclination angle of the pyramidal lattice trusses. For double-layered plates,  $h_1$  and  $h_2$  represent the core height of the top layer and the bottom layer,  $\alpha_1$  and  $\alpha_2$  represent the inclination angle of the pyramidal lattice trusses in the top and bottom layers, respectively.  $l$  is the bottom width of one pyramidal

unit cell, assumed to be identical for both single- and double-layered plates. Other geometrical parameters shown in Figure 1 are selected such that the single- and double-layered sandwich plates have the same total mass.

### Three-dimensional finite element model

The commercially available finite element package ANSYS is used to generate 3D meshes for both single- and double-layered sandwich plates, which are then transferred to the explicit integration version of the FE code LS-DYNA 971 R5.0 to carry out numerical simulations.<sup>22</sup>

To ensure numerical convergence, each double-layered plate is meshed with 10,38,637 elements, whilst the projectile is meshed with 5632 elements. The minimum element size is 0.56 mm for the projectile, 0.15 mm for pyramidal lattice trusses, 0.2 mm for the central ceramic prism directly under impact, 0.8 mm for the face-sheets, 0.48 mm for air, and 0.48 mm for the epoxy bonding layer, respectively. The region directly under projectile impact is modelled with relatively dense meshes to highlight the penetration details. To emulate the penetration process, ‘surface to surface eroding contact’ is employed to model the contacts between the sub-structures of the sandwich and the projectile. Contacts are updated once the elements on free surfaces of the structure are deleted according to relevant material failure criteria. A scale factor of 0.5 for sliding interface penalties is selected to define all the contacts.<sup>11</sup>

In the current study, the face-sheets, the lattice truss core and the projectile are made of AISI 304 stainless steel and modelled by the Johnson and Cook model with the consideration of strain rate effect, which has the form of

$$\sigma_y = (A + B\varepsilon_p^n)(1 + c\ln\dot{\varepsilon}^*)(1 - T^{*m}), \quad (1)$$

where,  $A$ ,  $B$ ,  $m$  and  $n$  are material constants with  $B$  and  $n$  representing strain hardening, and  $\varepsilon_p$  is the equivalent plastic strain. Further, the damage of the material element is defined as:

$$D = \sum \frac{\Delta\varepsilon^p}{\varepsilon^f} \quad (2)$$

where,  $\Delta\varepsilon^p$  is the increment of equivalent plastic strain and  $\varepsilon^f$  is the equivalent fracture strain for a given strain rate, temperature, pressure and equivalent stress. The Mie-Gruneisen equation of state model is used in conjunction with the Johnson and Cook model.<sup>22</sup>

For the ceramic (AD 98 alumina) prism insertions, the Johnson-Holmquist-Ceramics (JH-2) constitutive relation and fracture criterion are adopted,<sup>22</sup> which has been validated for describing the fracture behaviour of ceramics under high velocity penetration.<sup>11</sup> The model assumes that the strength of a ceramic is closely related with the exerting pressure, strain rate and damage. The damage is defined as the ratio of cumulative strain to failure strain and the relationship between the pressure and the specific heat capacity is included in the volume effect of the material. The JH-2

constitutive relation has the following form,

$$\sigma^* = \sigma_i^* - D(\sigma_i^* - \sigma_f^*), \quad (3)$$

where,  $\sigma_i^*$  is the intact, undamaged dimensionless effective stress,  $\sigma_f^*$  is the damaged dimensionless effective stress, and  $D$  is the damage parameter defined as:

$$D = \sum \frac{\Delta \varepsilon_p}{\varepsilon_p^f}, \quad (4)$$

where,  $\Delta \varepsilon_p$  represents an integration cycle of the material plastic strain and  $\varepsilon_p^f$  is the material breaking strain.

Due to the low strength of the void-filling epoxy compared with either steel or ceramic, it is regarded here as a kind of hydrodynamic material and modelled by applying the Elastic-Plastic-Hydro constitutive relation.<sup>23</sup>





The epoxy resin used for bonding has a mass density of 1185 kg/m<sup>3</sup>, shear modulus of 769 MPa and yield stress of 70 MPa. More details of the present FE model as well as material constitutive models and fracture criteria for AISI 304 stainless steel and AD 98 alumina can be found in Ni et al.,<sup>11</sup> and hence omitted here for brevity. The tensile modulus of the steel and ceramic mentioned here is 200 GPa and 386 GPa separately.

For single-layered plates, the FE model as described above has been successfully validated against experimental measurements.<sup>11</sup> In the present study, the FE model is firstly employed to assess how the double-layered sandwich construction favours over its single-layer counterpart in terms of ballistic protection and energy absorption capability under normal projectile impact, with further validation of the FE model performed by comparing the simulation results with experimental measurements of double-layered plates. Subsequently, as the oblique angle  $\varphi$  systematically increases, the variation trend of the penetration resistance is numerically predicted for double-layered plates and the underlying deformation/failure mechanisms are explored. The impact energy absorbed by each sub-component, the ballistic trajectory of the projectile with varying oblique angle, and the critical oblique angle are also calculated.

## Response of double-layered sandwich under normal ballistic impact

In this section, subjected to the constraint of equal total mass, the ballistic responses of three different kinds of double-layered sandwich plates are numerically simulated and compared with their single-layer counterpart that has been investigated experimentally and numerically by Ni et al.<sup>11</sup> Table 1 listed the key geometrical parameters associated with both the single- and double-layered sandwiches. Depending upon the value of core height ratio of  $h_1/h_2$ , the three double-layered sandwich specimens are referred below as sandwich 1, sandwich 2 and sandwich 3.

**Table 1.** Specifications and simulation results of single- and double-layered sandwich plates having pyramidal-ceramic-epoxy hybrid cores.

Sandwich No.	Schematic	$h_1/h_2$	$\alpha_1$ (°)	$\alpha_2$ (°)	$l$ (mm)	$H$ (mm)	$W$ (kg)	$V_b$ (m/s)
Single layer		–	50	–	29.3	17.5	1.08	~ 1300
1		0.5	28	43	29.3	22.1	1.08	~ 1630
2		1	37	37	29.3	22.1	1.08	~ 1780
3		2	43	28	29.3	22.1	1.08	~ 1850

$h_1/h_2$ : value of core height ratio;  $\alpha_1$ : inclination angle of the pyramidal lattice trusses in the top layer;  $\alpha_2$ : inclination angle of the pyramidal lattice trusses in the top and bottom layers;  $l$ : bottom width of one pyramidal unit cell;  $H$ : total height of sandwich plate;  $W$ : total weight of sandwich plate;  $V_b$ : ballistic velocity of sandwich plate.

### Experimental validation

Figure 2 illustrates schematically the experimental setup, with a ballistic rifle used to launch the impact projectile. A pair of brake screens spaced 300 mm apart and connected to a timing device is used to measure the projectile entry velocity. This is achieved by evaluating the ratio of screen spacing divided by the time difference between the moments separately triggered by the projectile impacting the first and second screens. In view of the drift effect in the process of projectile penetration through the sandwich, X-ray tomography is adopted to measure the exit velocity of the projectile. In a separate scheme, the exit velocity of the projectile is determined by evaluating the ratio of the distance between two projectile shadows in the X-ray native divided by the time difference between the two triggers.

For single-layer sandwich plates, the FE model has been successfully validated against experimental results in Figure 3(a) by Ni et al.<sup>11</sup> Figure 3(a) also shows that the ceramic single plate possesses similar ballistic performance with pyramidal-ceramic sandwich in the same weight. Pyramidal-ceramic sandwich occupies better resistance to the projectile as the initial velocity increases. To verify the accuracy of the present FE model predictions for double-layer sandwich plates, a series of experimental measurements with sandwich 2 specimens ( $h_1/h_2 = 1$ ) are carried out under normal ballistic impact conditions. The procedures and materials employed to fabricate the double-layer sandwich specimens as well as the experimental setup for measuring their ballistic responses are similar to those described in Ni et al. and they are hence not repeated here.<sup>11</sup> Representative single- and double-layer sandwich specimens are presented in Figure 1(a) and (b).

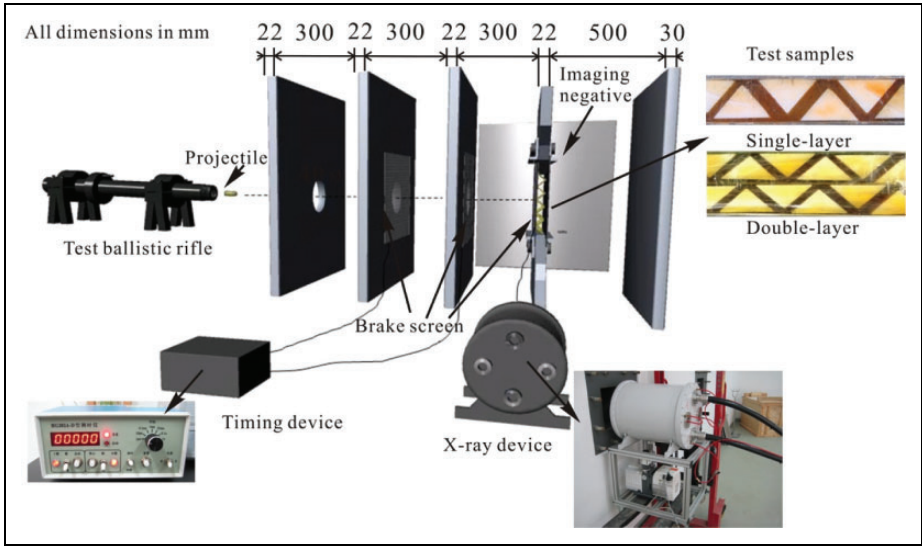


Figure 2. Experimental setup for measuring ballistic response of hybrid-cored sandwich plate.

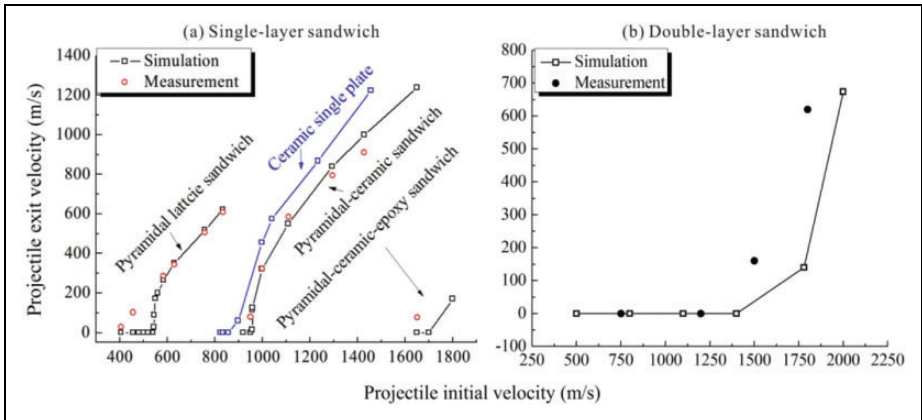


Figure 3. Projectile exit velocity plotted as a function of initial impact velocity for single layer sandwich (a) and double-layer sandwich 2 (b) (see Table 1 for definition): comparison between experimental measurements and FE simulations (FE simulation results for ceramic single plate which has the same weight with pyramidal-ceramic sandwich). FE: finite element.

For sandwich 2 specimens (see Figure 1 and Table 1) subjected to normal projectile impact, Figure 3(b) compares the experimentally measured projectile exit velocities with those calculated numerically for selected initial impact velocities. In general, the agreement between the test data and FE simulations is reasonable, thus validating further

the FE approach employed in the present study. The difference may be attributed to the complexities involved with the ballistic tests, the wobbly flying altitude of the projectile during the test, and the complicity associated with the 3D numerical simulations. Consequently, in the rest of this study, the FE model as described in Section 3 is employed to evaluate the ballistic performance of double-layer sandwiches and explore the underlying physical mechanisms. The numerically predicted ballistic limit velocities for the three double-layer specimens are summarized in Table 1; for comparison, the corresponding result for their single-layer counterpart having equal mass is also presented. Note that, at the ballistic limit velocity, the projectile just perforates the whole sandwich structure.

### *Deformation and failure modes*

In terms of ballistic limit velocity, the results of Table 1 show that all the three double-layered sandwich plates are considerably superior to their single-layer counterpart, with sandwich 3 enjoying a 42% increase over that of the latter (1850 m/s vs. 1300 m/s). It is worth noting that, also subject to the constraint of equal mass, Ni et al. demonstrated that the single-layered sandwich plate outperformed its monolithic counterpart.<sup>11</sup> In other words, for sandwich plates having pyramidal-ceramic-epoxy hybrid cores, the proposed concept of layered sandwich construction is beneficial so far as ballistic protection is of concern. Further, for double-layered constructions, the ballistic velocity increased as the value of  $h_1/h_2$  is increased. Consequently, to make better use of the layered sandwich construction, the mass of the hybrid core should be distributed more in the top layer facing first the strike of the impact projectile.

For the four different sandwich plates listed in Table 1, Figure 4(a)–(d) presented separately the numerically simulated deformation and failure modes under projectile normal impact at the ballistic limit velocity. For comparison, the experimentally observed failure configurations of sandwich 2 specimen after projectile penetration at the initial impact velocity of 1500 m/s are presented in Figure 4(e) and (f).

As shown in Figure 4(a), when the projectile is penetrating across the single-layer plate, the ceramic prisms directly taking the impact slows down the projectile whilst the stress wave spreads out from the central impact zone to the whole structure. The spreading is attributed mainly to the epoxy bonding effects between the truss members, the face-sheets and the ceramic prisms. Correspondingly, as a result of projectile penetration, apart from the central ceramic prism, the side ceramic prisms have also fractured. The small ceramic fragments are constrained by the epoxy resin, enabling further resistance to projectile penetration. Further, due to the epoxy bonding effects, the lattice truss members in the central impact zone deflects much less in comparison with those in single-layer sandwiches without void-filling epoxy, and the back face-sheet plays a more leading role in energy absorption than the front one (results not shown here for brevity). Towards the end of the penetration ( $\sim 90 \mu\text{s}$ ), the projectile is severely eroded by the central ceramic insertion. These results are consistent with those reported by Ni et al.<sup>11</sup> Compared to single AISI 304 stainless steel plate and ceramic-cored sandwich plate having the same total mass, Ni et al. also demonstrated that the



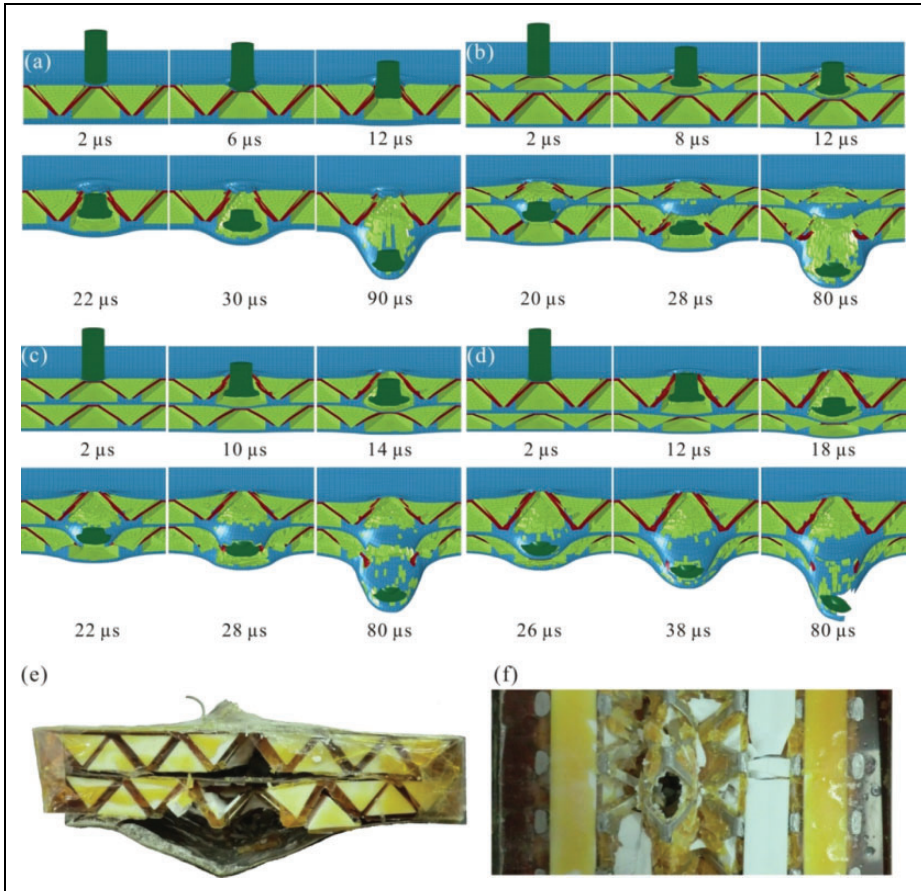


**Figure 4.** Evolution of deformation and failure under normal projectile impact at ballistic limit velocity: (a) single-layer sandwich (1300 m/s); (b) double-layer sandwich 1 (1630 m/s); (c) double-layer sandwich 2 (1780 m/s); and (d) double-layer sandwich 3 (1850 m/s). Experimentally observed failure modes of double-layer sandwich 2 under normal projectile impact at 1500 m/s. (e) Side view; (f) surface morphology of the bottom sandwich layer upon removing the bottom face-sheet. Euler elements for epoxy resin were marked for clarity.

single-layer sandwich with pyramidal-ceramic-epoxy core prolonged the penetration period of the projectile, so that each sub-structure of the hybrid-cored sandwich can deform and absorb the impact energy more sufficiently.<sup>11</sup>

The numerically predicted deformation and failure modes of the three double-layered sandwich plates are presented in Figure 4(b)–(d). Relative to their single-layer counterpart of Figure 4(a), the increased complexity of the double-layer configuration leads to increased interfacial complicacy, enabling more efficient energy absorption and stress wave deflecting/spreading. Upon perforating the top face-sheet at high speed, the

ballistic projectile rapidly enters the top sandwich layer. The ceramic insertions and the supporting metal lattice trusses absorb the impact energy by fragmentation and plastic deformation whilst the bottom sandwich layer acts as a load support. Simultaneously, the propagation speed of the projectile decelerates, accompanied by large deformation, abrasive erosion and mass loss. With further penetration, the middle face-sheet and the bottom sandwich layer start to absorb the remaining impact energy by plastic deformation and ceramic fragmentation. Due to the epoxy bonding effects, apart from the central ceramic insertions, the neighbouring ceramic insertions in both the top and bottom sandwich layers are also fragmentized. Further, subject to the constraint of equal mass, the results of Figure 4(b), (c) and (d) suggest that, as the value of  $h_1/h_2$  increases from 1/2 to 2, the ballistic velocity of the double-layer plate increases from 1630 m/s to 1850 m/s, implying that a thicker top layer relative to the bottom one is beneficial for ballistic protection. As the projectile completes its penetration across the top layer and starts to penetrate into the bottom layer, the metallic lattice trusses in the bottom layer are plastically deformed and fragmentation fracture occurs in some of the ceramic insertions. Thus, with a fixed total mass, increasing the thickness of the top layer while decreasing that of the bottom one improves the energy absorption capability of the whole structure. Consequently, under the present simulation conditions, sandwich 3 exhibits the best performance against ballistic perforation.

With reference to Figure 4(b), the projectile at a speed of 1630 m/s starts to penetrate the top layer of sandwich 1 at about 2  $\mu$ s. Its impact energy is absorbed by a multitude of mechanisms, including localized plastic deformation and perforation fracture of the top face-sheet, plastic deformation, bending flexure, fracture and node failure of the lattice truss members, and fragmentation fracture of the central ceramic insertion. At the same time, progressive erosion of the projectile occurs due to the presence of the ceramic insertion and its fragments (constrained by the surrounding epoxy bonding layer). At about 8  $\mu$ s, the middle face-sheet started to absorb the impact energy by plastic deformation even though the projectile tip is yet to reach it. At about 12  $\mu$ s, the projectile reaches the middle face-sheet, causing further deformation of the latter and initiating deformation/fracture of the lattice trusses and ceramic insertions in the bottom layer. At about 20  $\mu$ s, upon fully perforating the middle face-sheet, the projectile starts to penetrate the remaining sandwich structure. At about 28  $\mu$ s, the projectile penetrates into the bottom layer completely, interacting now directly with the central ceramic insertion and the supporting lattice truss members. Due to the continuing bending deformation of the middle face-sheet and the lateral spreading of stress waves, fragmentation fracture occurs in the side ceramic insertions whilst the bottom face-sheet start to deform plastically and deflect outwards. The projectile completes the penetration process across sandwich 1 at about 80  $\mu$ s, severely eroded, with only a small fraction of its initial mass left.

The predicted penetration process of the projectile at ballistic speed across sandwich 2 and 3 (see Figure 4(c) and (d)) is similar to that of sandwich 1 as described above, which agrees reasonably well with the experimentally observed failure configurations of sandwich 2 shown in Figure 4(e) and (f). One notable exception, however, is that, at about 38  $\mu$ s, even before the projectile fully perforates the middle face-sheet of

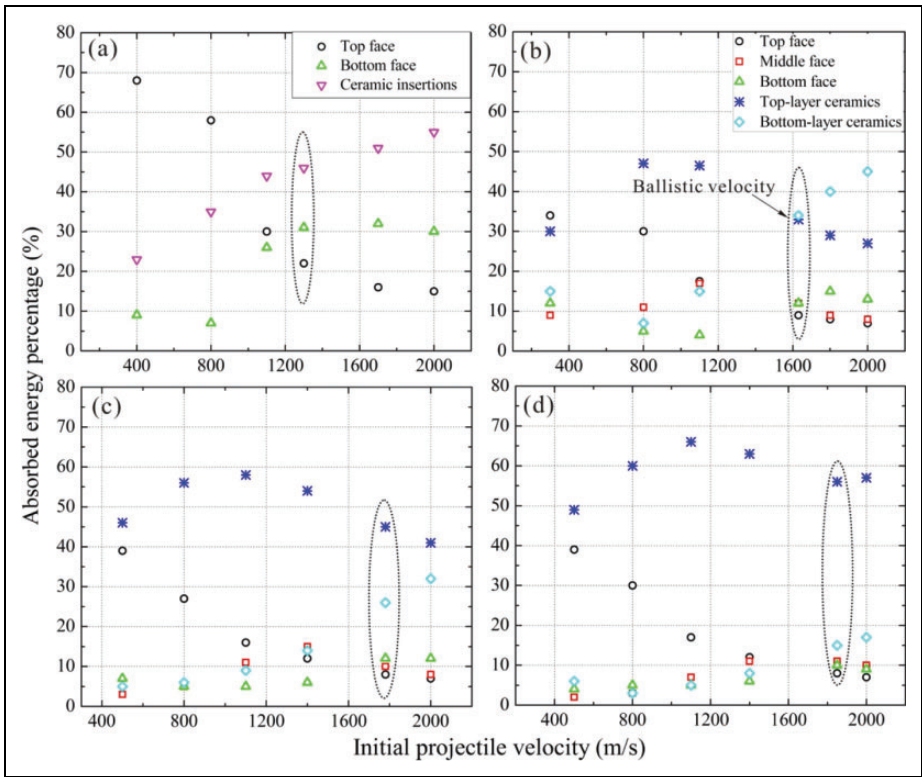


**Figure 5.** Energy absorption percentage of each sub-structure plotted as a function of initial project impact velocity for: (a) single-layer sandwich, (b) double-layer sandwich 1, (c) double-layer sandwich 2 and (d) double-layer sandwich 3.

sandwich 3, severe ceramic fragmentation occurs in the bottom layer although the projectile is yet to interact directly with the ceramic insertions in the bottom layer. The results of Figure 4(a)–(c) also suggest that, as the value of  $h_1/h_2$  increases from 1/2 to 2, the instant at which the projectile fully perforates the middle face-sheet is delayed, even though its initial impact velocity is increased from 1630 m/s to 1850 m/s.

### Energy absorption by sub-structures

For both single- and double-layer sandwich plates, the predicted energy absorption percentage is plotted in Figure 5 as a function of the initial projectile impact velocity. For clarity, only results for the main constituting elements (i.e. ceramic insertions and face-sheets) are presented, as the amount of energy absorbed by the lattice trusses and void-filling epoxy is relatively small. For the single-layer plate, the results shown in Figure 5(a) indicates that when the initial impact velocity is relatively small, the projectile interacts mainly with the upper portion of the sandwich: the amount of energy absorbed

by the top face-sheet via plastic deformation and perforation fracture is the highest, followed by the ceramic insertion directly under impact. As the initial velocity increases, whilst the amount of energy absorbed by the top face-sheet monotonically decreases, the percentage of energy absorbed by both the ceramic insertions and the bottom face-sheet gradually increases, each surpassing that absorbed by the top face-sheet at the ballistic velocity of  $\sim 1300$  m/s; see Figure 5(a).

As shown in Figure 5(b)–(d), when the initial velocity of the projectile impacting a double-layer plate is small (approximately 400 m/s), the energy absorption percentage of the ceramic insertions in the upper layer is comparable with that of the top face-sheet. However, as the initial velocity is increased, the ceramic insertions in the upper layer play a more leading role in energy absorption. This is attributed to the fact that, when the total mass of the double-layer plate is kept the same as that of its single-layer counterpart, the thickness of its three face-sheets decreases from 1.5 mm to 0.5 mm (Table 1), reducing therefore the amount of energy absorbed by the front face-sheet. As the initial velocity further increases, the percentage of energy absorbed by ceramic insertions in both the top and bottom layers increases, whilst that absorbed by the front face-sheet decreases.

For each double-layer plate considered, the energy absorbed by ceramic insertions in the top layer reached a maximum when the initial velocity is increased to about 1150 m/s (i.e. before the ballistic limit is reached). Below this velocity, the projectile interacts mainly with the front face-sheet and the constituting elements of the upper layer; when it penetrates into the bottom layer, its velocity is considerably decreased so that the energy absorption capability of the bottom layer is not efficiently utilized. However, as the initial velocity is increased beyond 1150 m/s, the residual velocity of the projectile entering the bottom layer is sufficiently high so that its main constituents can absorb enough amount of the remaining impact energy. As a result, the energy absorption percentage of both the ceramic insertions and the bottom face-sheet in the bottom layer increases, whilst that of the front face-sheet and top-layer ceramic insertions decreases; see Figure 5(b)–(d).

For all the three double-layer plates considered, the amount of energy absorbed by the top-layer ceramic insertions is always the highest at or below the ballistic velocity. When the bottom layer has a thickness twice that of the top one (i.e. sandwich 1), the maximum energy absorption percentage of the top-layer ceramic insertions is only about 45%. In contrast, for sandwich 3 having a top-layer thickness twice that of the bottom one, the maximum energy absorption percentage of the top-layer ceramic insertions is about 67%. As a result, the ballistic velocity of sandwich 3 is the highest, about 13% higher than that of sandwich 1 and 4% higher than that of sandwich 2.

It should be mentioned that the main focus of the present investigation is placed upon evaluating the concept of double-layer sandwich constructions with pyramidal-ceramic-epoxy hybrid cores for ballistic protection applications. Consequently, compared with single-layer plates having equal mass, the thickness of the face-sheets selected, 0.5 mm, is relatively small. As a result, as shown in Figure 5(b)–(d), the contribution of the face-sheets to total energy absorption is small, particularly at relatively high initial velocities. Also note that, as the initial velocity is increased, the percentage of impact energy

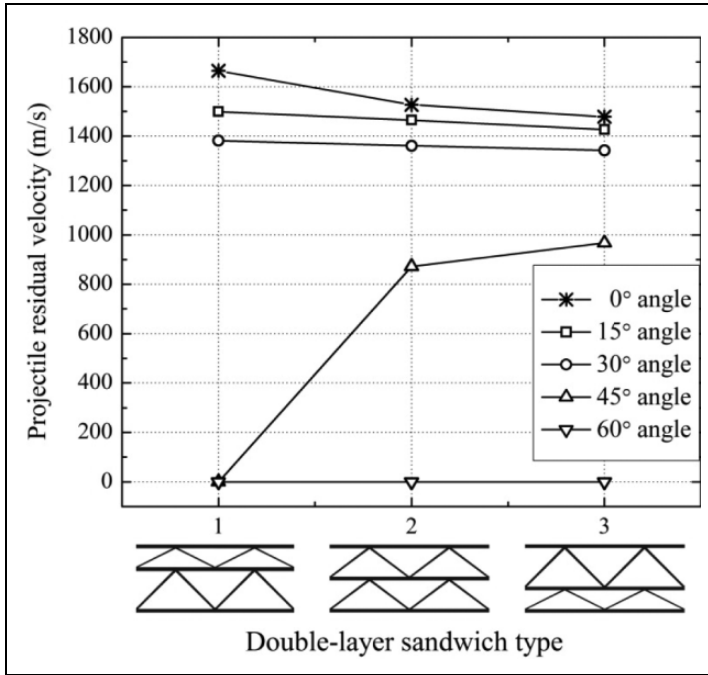


**Figure 6.** Numerically predicted residual velocity of impact projectile penetrating across double-layer sandwich plate at initial velocity of 2500 m/s for selected oblique angles.

absorbed by both the middle and bottom face-sheets increases, each surpassing that of the top face-sheet at the ballistic velocity.

## Response of double-layered sandwich under oblique ballistic impact

Consider next the ballistic responses of double-layer sandwich plates subjected to oblique projectile impact. To search for the critical oblique angle at which the projectile penetration process is changed from perforation to embedment, four oblique angles that is, 15°, 30°, 45° and 60° are selected, as shown schematically in Figure 1(d). For each oblique angle selected, the ballistic trajectory and erosion of the projectile, the deformation and failure modes of the sandwich structure, and the energy absorption percentage of each constituting element are calculated.

### Critical oblique angle

Figure 6 presents the predicted residual velocity of the impact projectile for selected oblique angles, with its initial velocity fixed at 2500 m/s. It is seen that the projectile with oblique angle equal to 0° (i.e. normal penetration with  $\varphi = 0^\circ$ ) had the strongest



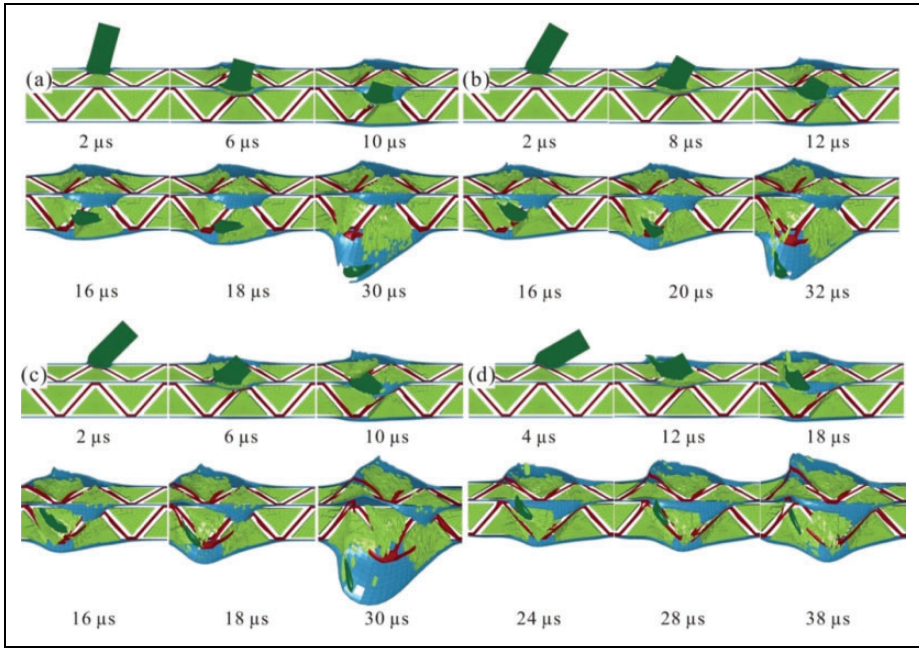


**Figure 7.** Evolution of deformation and failure in sandwich 1 under projectile impact at initial velocity of 2500 m/s for selected angles of obliquity: (a)  $\varphi = 15^\circ$ , (b)  $\varphi = 30^\circ$ , (c)  $\varphi = 45^\circ$  and (d)  $\varphi = 60^\circ$ . Euler elements for epoxy resin were marked for clarity.

penetration capability, achieving the highest residual velocity upon penetrating across the whole sandwich plate. For oblique angles equal to  $0^\circ$ ,  $15^\circ$  and  $30^\circ$ , the three double-layer plates exhibited similar performance, due mainly to the fact that the initial velocity of the projectile is sufficiently high (2500 m/s) so that its residual velocity is also high ( $>1300$  m/s). However, it could still be judged from Figure 6 that sandwich 3 exhibits the best ballistic protection performance, as the corresponding residual velocity is the smallest. On the other hand, for the case of  $\varphi = 45^\circ$ , an opposite trend is observed, with sandwich 1 now outperforming sandwich 2 and 3. For explanation, one is referred to the numerically simulated deformation and failure modes presented in Figure 7 for sandwich 1 under projectile impact at different oblique angles. From Figure 7(c) it is seen that, upon perforating the top face-sheet and entering the top layer of sandwich 1, the projectile at the oblique angle of  $45^\circ$  tends to move along the interfacial region between two neighbouring ceramic insertions. As a result, the energy absorption capability of the top layer is not fully exploited so that, for the case of  $\varphi = 45^\circ$ , the resistance of sandwich 1 to projectile penetration is dominantly attributable to the bottom layer. Given that the bottom layer of sandwich 1 is considerably thicker than that of sandwich 2 or sandwich 3, it may not be surprised that the critical oblique angle ( $45^\circ$ ) of sandwich 1 is smaller than that ( $60^\circ$ ) of sandwich 2 or sandwich 3.

## Deformation and failure modes

As a complement of Figure 6, the evolution of deformation and failure in sandwich 1 subjected to projectile impact at the initial velocity of 2500 m/s is presented in Figure 7 for varying angles of obliquity.

When the oblique angle is small ( $\varphi = 15^\circ$ ), upon entering the top layer, the tip of the projectile strikes firstly the sharp apex of the central ceramic prism, causing the latter to break into small fragment pieces; see Figure 7(a). At about 6  $\mu\text{s}$ , although the projectile is yet to perforate the middle face-sheet, the central ceramic prism in the bottom layer starts to fracture due mainly to the large bending deformation of the middle face-sheet. Subsequently, at about 10  $\mu\text{s}$ , the middle face-sheet is fully perforated, and the projectile now moves along the interstice between the central ceramic prism and the one located on its left. As the diameter of the projectile is much larger than the interstitial gap, the top portion of the two ceramic insertions break into small fragments to absorb the impact energy. Simultaneously, the small ceramic fragments are constrained by the surrounding epoxy bonding layer, which erodes the projectile to further resist its penetration. Upon penetrating into the bottom layer, the movement trajectory of the projectile is gradually shifted from the interstitial region back towards the central ceramic prism, causing the latter to completely break up. At about 30  $\mu\text{s}$ , the whole structure of sandwich 1 is fully perforated by the severely eroded projectile, see Figure 7(a).

For the case of  $\varphi = 30^\circ$ , it is seen from Figure 7(b) that the projectile entering the top layer interacts mainly with the central ceramic insertion, analogous to the case of  $\varphi = 15^\circ$  shown in Figure 7(a). However, different from the  $\varphi = 15^\circ$  case, once the projectile enters the bottom layer, it interacts mainly with the ceramic prism located on the left side of the central prism. Subsequently, with further penetration, the projectile is increasingly deflected back towards the interstice between the central prism and the one located on its left. To fully penetrate across the sandwich plate, the projectile now interacts with both ceramic prisms.

When  $\varphi = 45^\circ$ , once the projectile entered the top layer, its impact energy is absorbed by both the central ceramic prism and the one located on its left; see Figure 7(c). Upon entering the bottom layer, however, the left side prism adjacent to the central one plays a more dominant role in energy absorption and, correspondingly, its failure state is more serious than that of the latter. Subsequently, whilst the projectile penetrating across the left side prism is able to break up the prism located further away on the left, it is so eroded and decelerated that its remaining impact energy is not enough to fully perforate the bottom face-sheet even though the latter experiences large bending-dominated deformation. In other words, for sandwich 1,  $\varphi = 45^\circ$  may be taken as its critical oblique angle. Note also that, at  $\varphi = 45^\circ$ , the obliquity effect enhances the transverse ( $x$ -direction) movement of the projectile, reducing significantly its penetration capability in the vertical direction ( $y$  direction). The increasing transverse movement of the projectile with increasing oblique angle not only prolongs its interaction with the constituting elements of the sandwich but also leads to increased loss of its mass as well as impact energy due to erosion effects. Finally, it was seen from Figure 7(c) that, significantly different from the cases shown in Figure 7(a) and (b) for relatively small

oblique angles, the projectile at the critical oblique angle of  $45^\circ$  forces not only the middle face-sheet to hump upwards but also localized fragment fracture of the second left ceramic prism in the top layer.

As shown in Figure 7(d), with its oblique angle equal to  $\varphi = 60^\circ$ , the projectile entering the top layer moves along the interstice between the central prism and the one located on its left, forcing both to break into small fragments. Constrained by the epoxy bonding layer, these small fragments in turn causes serious erosion of the projectile, reducing significantly its mass. The projectile then perforates the middle face-sheet and interacts mainly with the ceramic prism located on the left side of the central one. Subsequently, with further penetration, the gravely eroded and much decelerated projectile starts to fracture the second left ceramic prism but cannot complete the process as its velocity is eventually reduced to zero. The transverse movement trajectory of the projectile is analogous to the case of critical oblique angle ( $\varphi = 45^\circ$ ) shown in Figure 7(c): the penetration stops within the second left ceramic prism, with localized fracture initiated in the prism located further left. However, relative to the case of  $\varphi = 45^\circ$ , the fragmentation fracture of the ceramic prism located to the immediate left of the central one is more serious than the latter, absorbing therefore more impact energy. In addition, it is seen from Figure 7(d) that the deformation of the sandwich plate as a whole as well as its vertical bending deformation (humping downward) are less significant than those shown in Figure 7(c).

The penetration process of the projectile having varying oblique angles across either sandwich 2 or sandwich 3 is similar to that described above for sandwich 1 and hence not be repeated here. However, it is established that, rather than  $\varphi = 45^\circ$ , the critical oblique angle for both sandwich 2 and sandwich 3 is  $\varphi = 60^\circ$ . Further, in comparison with a homogeneous steel plate of equal mass, ricochet rarely occurs in the present single- or double-layer sandwich plates with hybrid-cores as their relatively thin top face-sheet enables the projectile to perforate with ease. Also, embedment is more likely to occur in the hybrid-cored sandwiches in comparison with the monolithic plate.

### *Residual mass and transverse movement trajectory of impact projectile*

To explore further the mechanisms underlying the penetration process of the projectile having different oblique angles, Figure 8(a), (c) and (e) plot  $m/M$  as a function of projectile movement trajectory ( $y$  direction) whilst Figure 8(b), (d) and (f) plot  $2x/l$  as a function of  $y/H$  for the three double-layer plates considered. Again, the projectile initial impact velocity is fixed at 2500 m/s. Here, with reference to Figure 1,  $2x/l$  and  $y/H$  denote the non-dimensional  $x$ - and  $y$ -direction coordinates of the projectile tip during penetration,  $l$  and  $H$  being the pyramidal unit cell width and total sandwich height, respectively, and  $m/M$  denotes the ratio of projectile residual mass to initial mass.

For all the three double-layer sandwich plates considered, it is seen from Figure 8 that, for a given  $y$ -position of the projectile, its residual mass decreases whilst its transverse movement increases as the oblique angle is increased. In particular, the projectile with  $\varphi = 45^\circ$  or  $\varphi = 60^\circ$  advances the farthest along the  $x$ -direction (i.e. transverse direction) in comparison with smaller oblique angles, and hence its interaction with the constituting elements of the double-layer plate is the most intensive. Further, the farthest vertical



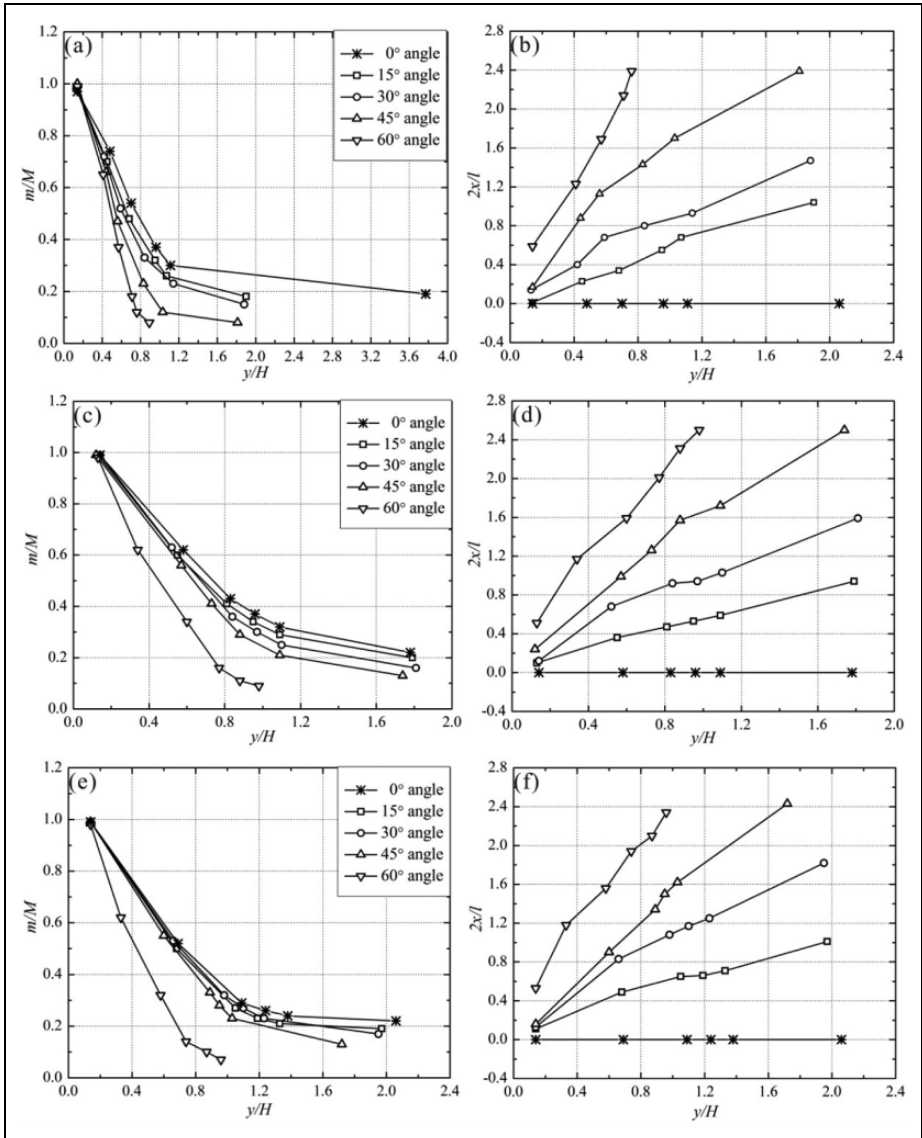


**Figure 8.** Effect of oblique angle on ratio of projectile residual mass to initial mass ( $m/M$ ) and projectile movement trajectory for double-layer sandwich plates: (a and b) sandwich I; (c and d) sandwich 2; (e and f) sandwich 3.  $2x/l$  and  $y/H$  denoted non-dimensional x- and y-direction coordinates of projectile tip during penetration,  $l$  and  $H$  being pyramidal unit cell width and total sandwich height, respectively (see Figure 1). Projectile initial impact velocity fixed at 2500 m/s.

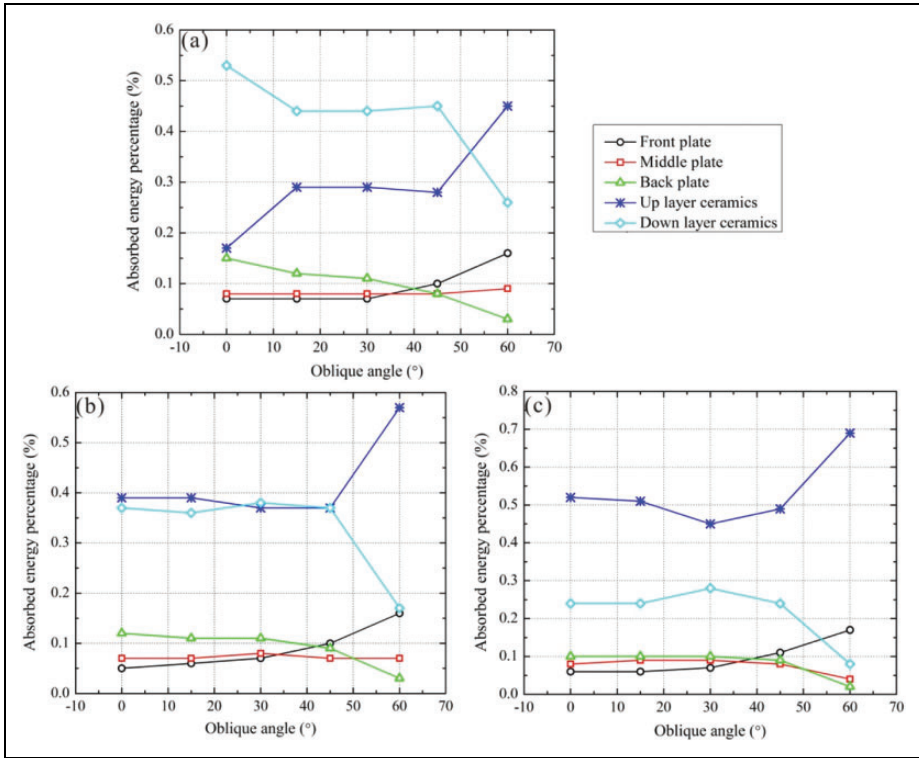


**Figure 9.** Energy absorption percentage of key constituting elements plotted as a function of oblique angle with projectile initial impact velocity fixed at 2500 m/s for double-layer plates: (a) sandwich 1; (b) sandwich 2; and (c) sandwich 3.

position that the projectile can move to decrease with increasing oblique angle. Correspondingly, the resistance of the sandwich to projectile penetration increases with increasing oblique angle. Note that the farthest transverse position a projectile with  $\varphi = 45^\circ$  can achieve, about  $1.25l$ , is nearly the same as that of the projectile with  $\varphi = 60^\circ$ . At these relatively large oblique angles, the penetration capability of the projectile is gravely weakened due to a large mass loss associated mainly with the strong erosion effects of the ceramic prisms.

The results of projectile residual mass and trajectory movement shown in Figure 8(a) and (b) for sandwich 1 are noticeably different from those of Figure 8(c)–(f) for sandwich 2 and 3. This is attributable to the fact that the former has a critical oblique angle of  $\varphi = 45^\circ$  whilst the latter had  $\varphi = 60^\circ$ .

### Energy absorption by constituting elements

To compare the efficiency of impact energy absorption among the double-layer sandwich plates as listed of Table 1, Figure 9 plots the energy absorption percentage of key

constituting elements as a function of oblique angle (initial impact velocity fixed at 2500 m/s). The results of Figure 9 indicate that ceramic prism insertions play a more dominant role in absorbing the impact energy than the three face-sheets. For the configuration of sandwich 1 ( $h_1/h_2 = 0.5$ ), both the mass and height of its top layer are smaller than those of the bottom one. It is not surprising therefore that the energy absorption performance of the top-layer constituting elements is inferior to that of the bottom-layer ones when the oblique angle is  $0^\circ$ ,  $15^\circ$ ,  $30^\circ$  or  $45^\circ$ ; respectively, see Figure 9(a). For the case of an oblique angle equal to  $60^\circ$ , however, the transverse movement of the projectile is so significant that embedment occurs. The penetration of the projectile occurs mainly in the interfacial region between the top and bottom layers. The humping movement of the middle face-sheet towards the upper left causes further fragmentation of the ceramic prisms in the top layer even though the projectile has already penetrated into the bottom layer; see Figure 7(d). Consequently, in this case, the amount of energy absorbed by the top-layer ceramic prisms exceeds that of the bottom-layer ones.

As to sandwich 2 ( $h_1/h_2 = 1$ ), the mass and height of its top layer are identical to those of its bottom layer. As a result, the ceramic prisms in the top layer absorbs nearly the same amount of energy as that absorbed by the bottom-layer ones for oblique angles equal to or less than  $45^\circ$ ; see Figure 9(b). As the oblique angle is increased to  $60^\circ$ , similar to that described above for sandwich 1, the humping of the middle face-sheet towards the upper left during the latter stage of the penetration process increases significantly the amount of energy absorbed by the top-layer ceramic prisms.

The energy absorption performance of sandwich 3 ( $h_1/h_2 = 2$ ) is similar to sandwich 2, except that the ceramic prisms in the top layer (twice thicker than the bottom layer) always plays the dominant role irrespective of the projectile oblique angle. As a result, sandwich 3 exhibits the best ballistic protection performance under all the oblique angles considered.

## Concluding remarks

The concept of double-layer sandwich construction with metallic pyramidal lattice-ceramic insertions-epoxy filling hybrid core for ballistic protection is evaluated using 3D finite element simulations. Both normal and oblique projectile impact conditions are considered. The numerical predictions are successfully validated by comparing with results measured experimentally using ballistic rifle. It is demonstrated that, under the present simulation conditions, the ballistic protection performance of the proposed double-layer sandwich plate is superior to its single-layer counterpart of equal mass, with the former achieving a ballistic limit velocity of about 1850 m/s under normal projectile impact whilst that of the latter is only about 1300 m/s. The presence of the ceramic insertions causes serious erosion and mass loss of the projectile, whilst the void-filling epoxy resin contributes to further enhance the ballistic resistance of the hybrid-cored sandwich by adhering its constituting elements as an integrated whole.

Subject to the constraint of equal mass, increasing the height (and hence mass) of the top layer facing the initial strike of the impact projectile enhances the ballistic protection capability of the double-layer sandwich. Increasing the angle of obliquity leads to

increased transverse movement of the projectile, which in turn prolongs its interaction with the constituting elements of the hybrid core. As a result, the erosion effects of the ceramic insertions on the penetrating projectile intensifies, causing more serious loss of its mass. In comparison with homogeneous (monolithic) metal plates, ricochet rarely occurs in the present double-layer sandwich plates as their relatively thin top face-sheet enables the projectile to perforate with ease. Also, embedment is more likely to occur in the hybrid-cored sandwiches in comparison with monolithic plates, especially at large oblique angles.

The results presented here would be helpful for designing lightweight layered constructions having superior ballistic protection capabilities. Future research is needed to investigate a number of issues not addressed in the present study, including the influence of face-sheet thickness, the position of projectile impact, and the penetration resistance of the hybrid-cored sandwich to multiple projectile impacts.

### Declaration of Conflicting Interests

The author(s) declared no potential conflicts of interest with respect to the research, authorship, and/or publication of this article.

### Funding

The author(s) disclosed receipt of the following financial support for the research, authorship, and/or publication of this article: This work was financially supported partially by the National Basic Research Program of China (2011CB6103005), partially by the National 111 Project of China (B06024), partially by National Natural Science Foundation of China (11472208) and partially by the Shaanxi Province 13115 Project. The authors gratefully acknowledge the support by the opening project (project number KFJJ13-11 M) of State Key Laboratory of Explosion Science and Technology (Beijing Institute of Technology) and the open fund SV2014-KF-17 of State Key Laboratory for Strength and Vibration of Mechanical Structures.

### References

1. Bruce KF. Performance metrics for composite integral armor. *J Thermoplast Compos* 2000; 13: 417–431.
2. Almohandes AA, Abdel-Dader MS and Eleiche AM. Experimental investigation of the ballistic resistance of steel-fiberglass reinforced polyester laminated plates. *Compos B-Eng* 1996; 27B: 447–458.
3. Gupta NK and Madhu V. An experimental study of normal and oblique impact of hard-core projectile on single and layered plates. *Int J Impact Eng* 1997; 19: 395–414.
4. Teng X, Wierzbicki T and Huang M. Ballistic resistance of double-layered armor plates. *Int J Impact Eng* 2008; 35: 870–884.
5. Ashby MF, Evans AG, Fleck NA, et al. *Metalfoam: a design guide*. London: Butterworth-Heinemann, 2000.
6. Banhart J, Ashby MF and Fleck NA. Metal foams and porous metal structures: *1st International Conference on Metal Foams and Porous Metal Structures* (eds Banhart J, Ashby MF and Fleck NA), Bremen, Germany, 14–16 June 1999, MIT.

7. Evans AG, Hutchinson JW and Ashby MF. Multifunctionality of cellular metal systems. *Prog Mater Sci* 1998; 43: 171–221.
8. Gibson LJ and Ashby MF. *Cellular Solids: Structure and Properties*. 2nd ed. Cambridge: Cambridge University Press, 1997.
9. Wadley HNG, Fleck NA and Evans AG. Fabrication and structural performance of periodic-cellular metal sandwich structures. *Compos Sci Technol* 2003; 63: 2331–2343.
10. Yungwirth CJ, Radford DD, Aronson M, et al. Experiment assessment of the ballistic response of composite pyramidal lattice truss structures. *Compos B-Eng* 2008; 39: 556–569.
11. Ni CY, Li YC, Xin FX, et al. Ballistic resistance of hybrid-cored sandwich plates: numerical and experimental assessment. *Compos A-Appl S* 2013; 46: 69–79.
12. Bazle ZH and John WGJ. A combined theoretical-semiempirical penetration model of ballistic penetration of thick section composites. *J Thermoplast Compos* 2012; 25: 632–659.
13. Shanazari H, Liaghat GH, Hadavinia H, et al. Analytical investigation of high-velocity impact on hybrid unidirectional/woven composite panels. *J Thermoplast Compos*. Epub ahead of print 16 September 2015. DOI: 10.1177/0892705715604680.
14. Tasdemirci A and Tunusoglu G. Experimental and numerical investigation of the effect of interlayer on the damage formaton in a ceramic/composite armor at a low projectile velocity. *J Thermoplast Compos*. Epub ahead of print 7 May 2015. DOI: 10.1177/0892705715584410.
15. Tasdemirci A and Kara A. The effect of perforatons on the stress wave propagation characteristics of multilayered materials. *J Thermoplast Compos*. Epub ahead of print 7 May 2015. DOI: 10.1177/0892705715584409.
16. Backman EM and Goldsmith W. The mechanics of penetration of projectiles into targets. *Int J Eng Sci* 1978; 16: 1–99.
17. Johnson W, Sengupta AK and Ghosh SK. High velocity oblique impact and ricochet mainly of long rod projectiles: an overview. *Int J Impact Eng* 1982; 24: 425–436.
18. Corbett GG, Reid SR and Johnson W. Impact loading of plates and shells by free-flying projectiles: a review. *Int J Impact Eng* 1996; 18: 141–230.
19. Goldsmith W. Non-ideal projectile impact on targets. *Int J Impact Eng* 1999; 22: 95–395.
20. Awerbuch J, Bodner SR and Johnson W. An investigation of oblique perforation of metallic plates by projectiles. *Exp Mech* 1977; 17: 147–153.
21. Børvik T, Olovsson L, Dey S, et al. Normal and oblique impact of small arms bullets on AA6082-T4 aluminium protective plates. *Int J Impact Eng* 2011; 38: 577–589.
22. Livermore Software Technology Corporation, California, USA, LS-DYNA 970, 2005.
23. Lopez-Puente J, Arias A, Zaera R, et al. The effect of the thickness of the adhesive layer on the ballistic limit of ceramic/metal armours: an experimental and numerical study. *Int J Impact Eng* 2005; 32: 321–336.